Batteries & Supercaps

Research Article
doi.org/10.1002/batt.202400307

Chemistry Europe
European Chemical Societies Publishing

www.batteries-supercaps.org

Highly Effective Electrolytes Toward High-Performance Aluminum/Seawater Batteries

Qingchao Xia[+],[a, b] Zhengnan Li[+],[a, c] Dewei Liu[+],[a, b] Nan Song,[a, c] Nan Zhang,[c] Shuyang Ma,[a, b] Zeliang Wu,*[a, b] and Weiyong Yuan*[a, d]

The poor performance of metal/water batteries caused by self-corrosion of anodes and low catalytic activity of cathodes has been a long-standing challenge, greatly limiting their practical applications, in particular the underwater unmanned vehicle (UUV) application. We have fabricated an Al/seawater battery using simulated seawater with an appropriate pH and added with polyacrylic acid (PAA) as the electrolyte. This electrolyte simultaneously greatly retards self-corrosion of the Al anode by *in situ* forming a PAA-Al^{3+} complex film on it and increases the electrocatalytic activity toward the hydrogen evolution reaction by improving the electronic structure of Pt. When utilizing the multielement-doped Al sheet as the anode and nickel foam supported loading-amount-optimized Pt/C catalyst as the cathode and adopting the developed new electrolyte, the obtained Al/H_2O battery exhibits an energy density of 2271 Wh kg^{-1}, which is the highest among those of all the reported batteries, and a power density of 20.87 mW cm^{-2}, which outperforms all the reported metal/H_2O batteries. This work not only develops a new type of high-performance Al/H_2O batteries for practical applications such as UUVs, but provides scientific insight into the design of superior electrolytes, which could be further extended for improving the performances of various metal batteries.

Introduction

In recent years, underwater unmanned vehicles (UUVs) have developed rapidly, demonstrating practical applications including seafloor mapping, ocean current characterization, and marine life monitoring. In the civil field, UUVs are frequently used for disaster relief and oil and gas exploration; in the military field, UUVs can carry various sensors for data collection, surveillance, and reconnaissance.[1] Lithium batteries are conventionally employed to power the UUVs, but their energy densities are relatively low, and will be further reduced when applied to the deep sea because of the need to use pressure-resistant shells.[2] This greatly compromises the endurance of UUVs. In addition, further increasing the energy density of lithium batteries may cause safety issues; the thermal runaway at high power output may even lead to explosion. Therefore, it is critical to fabricate electrochemical energy devices possessing high energy density and able to work safely and stably in the marine environment for addressing the energy challenges involved in UUVs.

Al batteries could be highly promising as power sources for UUVs because Al is abundant and inexpensive with a theoretical capacity density of 2.98 Ah g^{-1}, and an energy density of 8.1 Wh g^{-1},[3] which is the highest among the commonly used materials for power generation, and it has good electrochemical activity in seawater.[4] Several types of these batteries have been explored, including Al/MnO_2,[5] Al/AgO,[6] Al/H_2O_2,[7] and Al/air ones.[8] However, the discharge times of these batteries are relatively short. In addition, additional oxidants are required, making the battery fabrication more complicated, and increasing the cost. It remains extremely challenging but highly desirable to develop Al-based batteries with high anode utilization efficiency, high energy density, high power density, easy fabrication, and low cost for practical UUV applications.

Al/H_2O batteries consume only water and Al anodes, require no additional oxidizer, and generate environmentally friendly reaction products. The main reactions of the aluminum-water cell are:

$$\text{Anode reaction}: \quad Al + 3OH^- \rightarrow Al(OH)_3 + 3e^- \tag{1}$$

$$\text{Cathodic reaction}: \quad 2H_2O + 2e^- \rightarrow H_2 + 2OH^- \tag{2}$$

Due to the easy availability of water, Al/H_2O batteries also hold particular promise in marine environments. Nevertheless, there are still great challenges to create high-performance Al/H_2O batteries from both the anode and cathode sides: for the Al

[a] *Dr. Q. Xia,[+] Z. Li,[+] D. Liu,[+] N. Song, S. Ma, Z. Wu, Prof. W. Yuan*
Ningbo Innovation Center
Zhejiang University
Ningbo 315100, China
E-mail: wyyuan@zju.edu.cn

[b] *Dr. Q. Xia,[+] D. Liu,[+] S. Ma, Z. Wu*
College of Mechanical Engineering
Zhejiang University
Hangzhou 310027, China
E-mail: wuzeliang@zju.edu.cn

[c] *Z. Li,[+] N. Song, N. Zhang*
College of Mechanical Engineering
Yanshan University
Qinhuangdao 066004, China

[d] *Prof. W. Yuan*
College of Chemical and Biological Engineering,
Zhejiang University
Hangzhou 310027, China

[+] *These authors contributed equally to this work.*

Supporting information for this article is available on the WWW under https://doi.org/10.1002/batt.202400307

Research Article
doi.org/10.1002/batt.202400307
Chemistry Europe
European Chemical Societies Publishing

anode, it is frequently passivated by Al_2O_3 formed naturally on Al and/or $Al(OH)_3$ produced during the battery operation,[9,10] and can spontaneously react with H_2O to produce H_2 to reduce the utilization efficiency of Al;[11] for the cathode, the hydrogen evolution reaction (HER) occurring on this electrode is sluggish,[12] limiting the power output of the Al/H_2O batteries. Therefore, it is highly crucial to simultaneously activate the Al anode, improve the utilization of Al, and increase HER catalytic efficiency for enhancing their performance. Currently, there are two reported studies developing Al/H_2O batteries.[13,14] However, none of them are focused on simultaneously improving the activation and self-corrosion of Al and HER activity of the cathode, and the energy density and power density are quite low, which greatly limit further development of this battery technology and make it elusive to realize the applications of these batteries.[13,14]

Modification of seawater by adjusting its pH and adding self-corrosion inhibitors could not only employ the advantages of seawater for UUV applications, but modulate the dissolution of surface oxide layer and inhibit the self-corrosion, thus improving the oxidation kinetics and utilization of the anode.[15–18] In addition, the inhibitor could interact with the cathode catalysts to enhance the HER activity.[19,20] In this work, we have fabricated structurally simple Al/H_2O batteries using pure Al as the anode, Pt/C coated nickel foam (NF) (NF@Pt/C) as the cathode, and a new electrolyte, which uses simulated seawater with an appropriate pH and added with polyacrylic acid (PAA) as the self-corrosion inhibitor. The effect of PAA concentration on the battery performance was systematically explored and the mechanism was studied. To further enhance the performance for practical applications, an Al/H_2O battery was fabricated using an anode made of multi-element-doped Al, a cathode with optimized Pt/C loading, and the optimized electrolyte. Its performance was further tested.

Results and Discussion

The pH Optimization of Simulated Seawater

The activation and utilization of Al are highly dependent on the pH of the electrolyte. The pH of the simulated seawater was adjusted to improve the performance of the Al anode. The polarization curves of the fabricated Al/H_2O batteries were tested in the simulated seawater with pH 7, 12, and 14. The power density of Al/H_2O battery in the pH 12 electrolyte was significantly higher compared to that in the neutral one (Figure 1). This is due to OH^- under the alkaline condition dissolving the surface oxidation layer and/or formed $Al(OH)_3$ more easily to activate the Al anode.[21] However, at pH 14, the anode efficiency is significantly lower than that at pH 12. This is caused by the too fast chemical reaction between Al and OH-, which greatly reduces the electrochemical utilization of Al for producing electricity. Therefore, all the following tests were carried out using simulated seawater with pH adjusted to 12 as the electrolyte.

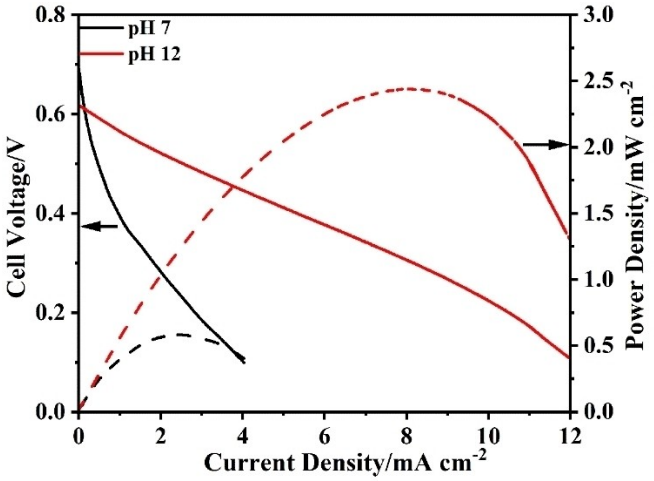

Figure 1. Polarization curves and corresponding power density curves of Al/H2O batteries in the simulated seawater with PAA at pH 7 and 12.

The Influence of PAA Addition in the Electrolyte on Al Utilization

To further improve the anode efficiency, while still keeping the anode highly active, PAA was added to the simulated seawater (pH adjusted to 12) to produce a new electrolyte of the Al/H_2O battery. Figure 2 shows the utilization efficiency of the anode at different PAA concentrations. The anode utilization efficiency significantly increases from 47.26% to 59.92% when PAA with a concentration of 0.05 mg mL^{-1} is introduced; with increase of the PAA concentration to 0.1 mg mL^{-1}, the anode efficiency slightly decreases to 54.79%; this efficiency keeps essentially unchanged when further increasing the PAA concentration to 0.3 mg mL^{-1}. Therefore, PAA reduces self-corrosion of the Al anodes.

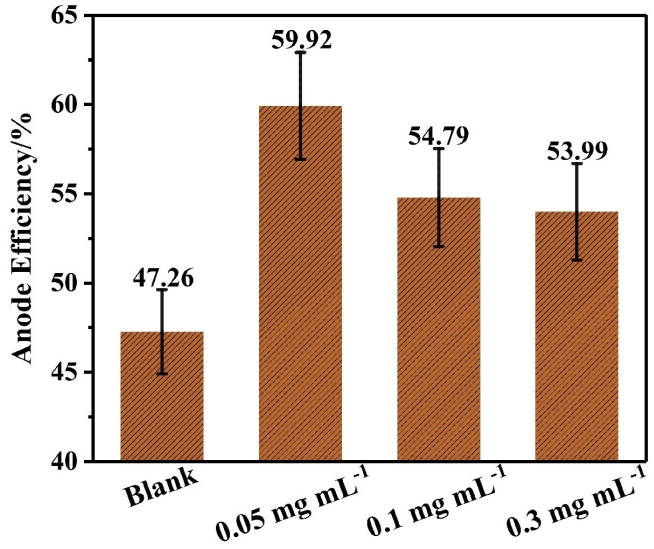

Figure 2. Anode efficiencies of the Al anodes in Al/H_2O batteries measured in simulated seawater without PAA and with PAA at different concentrations at pH 12.

Research Article
doi.org/10.1002/batt.202400307
Chemistry Europe
European Chemical Societies Publishing

In order to further investigate the self-corrosion inhibition effect of PAA, the anodes of Al/H_2O batteries discharged in 0.1 mg mL^{-1} PAA-added alkaline electrolyte with a current density of 2 mA cm^{-2} for different time intervals were investigated (the anodes are denoted as Al–C-PAA) (Figure 3E–H). For comparison, the anodes after the same discharge time in electrolyte without PAA were also studied (denoted as Al–C) (Figure 3A–D). After discharged for 2 h, a lot of pores can be observed on Al–C (Figure 3A). Their sizes are 100 nm. On the other hand, the surface of Al–C-PAA is quite smooth with no pores on it (Figure 3E). The large particles (the bright area) are probably caused by incomplete corrosion of the surface oxidation layer of Al (Figure 3E). With the increase of the discharge time to 4 h, the size of pores on Al–C significantly increases to 180 nm, and the neighbouring pores coalesce, leading to a reduced density (Figure 3B). However, only a few ultrasmall pores with sizes of 20 nm are observed on the surface of Al–C-PAA (Figure 3F). When the discharge time is increased to 6 h, the size of pores on Al–C further drastically increases to 250 nm, and these pores coalesce to result in a further reduced density (Figure 3C). For Al–C-PAA, numerous ultrasmall pores appear on its surface, and their size is 25 nm, which is only slightly higher than that 20 mm (Figure 3G). When the discharge time is 8 h, the pore size increases even more, and no clear boundaries between pores are observed at this magnification (Figure 3D). Nevertheless, the pores on Al–C-PAA have a size of 25 nm, similar to that at 6 h, although their density greatly increases (Figure 3H). The morphology evolution clearly shows that the addition of PAA can significantly slow down the corrosion process. This result further confirms that PAA in the electrolyte inhibits the self-corrosion of the Al anode.

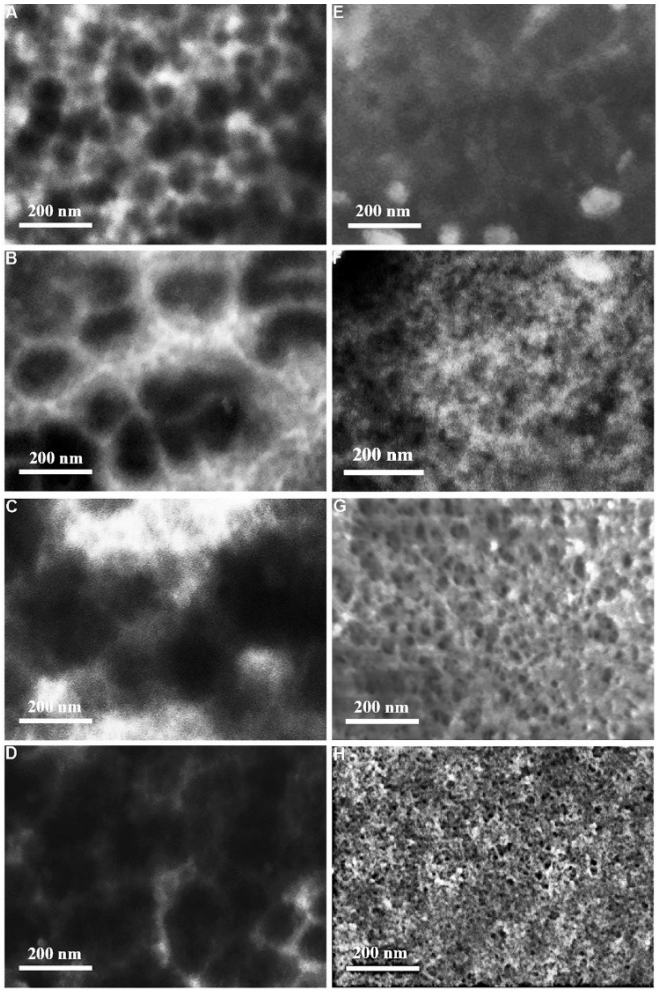

Figure 3. FESEM images of Al anodes discharged for 2 h (A, E), 4 h (B, F), 6 h (C, G), and 8 h (D, H) in 3.5 % NaCl solution at pH 12 without (A–D) and with (E–H) 0.1 mg mL^{-1} PAA.

Mechanism for PAA-Inhibited Self-Corrosion of Al Anode

In order to explore the mechanism for the inhibition of self-corrosion, we used EDX mapping to investigate the surface elemental composition and distribution of Al–C-PAA (Figure 4). The images of C, O, and Al elements show that they are uniformly distributed on the surface of the Al anode (Figure 4C–E). This is further demonstrated via the overlapping image (Figure 4B). This result suggests the formation of a PAA-Al^{3+} complex film on the anodes. The EDX analysis result (Figure 4F) further indicates that a PAA-Al^{3+} complex film has been formed on the surface of the Al anode. The surface distribution of PAA-Al^{3+} complexes after discharge at current density of 5 mA cm^{-2} for 10 h was also checked via the EDX mapping (Figure S1). The SEM image (Figure S1A) shows that the Al anode is still smooth with no large pores. The mapping images (Figure S1B–E) reveal

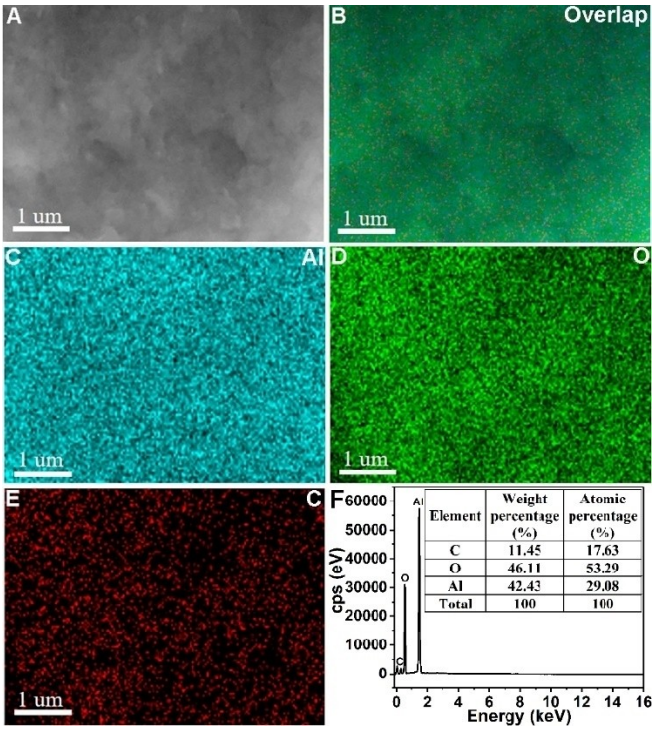

Figure 4. SEM image (A), EDX mapping images (B–E), and EDX analysis (F) of the Al anode after discharge at 2 mA cm^{-2} for 10 h in 0.1 mg mL^{-1} of PAA-added alkaline electrolyte. (B) is the overlapping image. (C), (D), and (E) show distribution of Al, O, and C, respectively.

Research Article
doi.org/10.1002/batt.202400307
Chemistry Europe
European Chemical Societies Publishing

that the PAA-Al^{3+} complexes are also uniformly distributed on the Al anode.

To further reveal the chemical composition of the surface layer, the FTIR spectroscopy of this anode was carried out. The FTIR spectrum of PAA is also displayed for comparison (Figure 5). A broad peak corresponding to the O–H stretching vibrations of -COOH in PAA is observed in the range 3000–3500 cm^{-1}.[22] In the case of PAA–Al^{3+}, the broad band appears in a similar region between 3000–3600 cm^{-1}. The band at 1715 cm^{-1} in the spectrum of PAA corresponds to stretching vibrations of the carbonyl group in PAA.[22] However, in the spectrum of PAA-Al^{3+}, a new band of low intensity appears at 1635 cm^{-1}, which is ascribed to stretching asymmetric vibration of the ionized carboxyl group.[22] Relative intensity of the peak at 1456 cm^{-1} in the PAA-Al^{3+} spectrum sharply increases as compared to that in the PAA spectrum, further confirming the formation of the PAA-Al^{3+} complexes.[22]

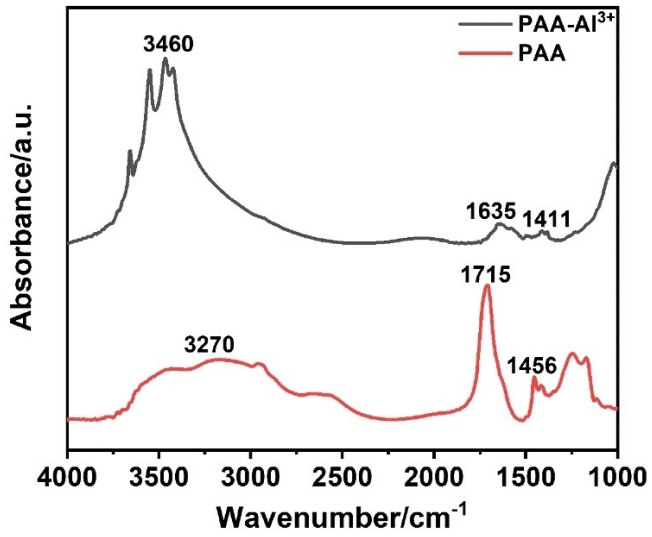

Figure 5. FTIR spectra of PAA and PAA-Al^{3+}.

During the operation of the Al/H_2O battery, the Al anode loses electrons to the Pt/C cathode through the external circuit for HER. The OH^- and deprotonated PAA will be competitively adsorbed on the Al^{3+} produced in the anode via electrostatic interaction and coordination bonding.[22,23] Due to its multivalency, PAA has stronger adsorption capability compared to OH^-. In addition, since a single polymer chain displaces many water molecules from the metal surface, the adsorption of PAA on the Al anode is entropically favorable.[23,24] The *in situ* formed PAA-Al^{3+} complex film reduces the surface area of Al in direct contact with the electrolyte, thus protecting the anode and increasing its efficiency. The mechanism for the corrosion inhibition effect of PAA is illustrated in Figure 6.

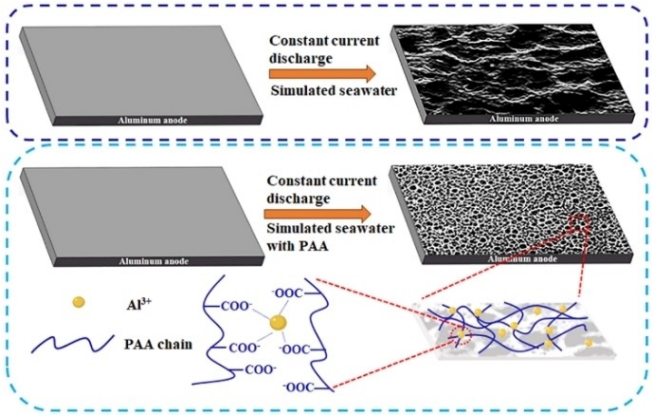

Figure 6. Schematic illustration of the mechanism for the corrosion inhibition effect of PAA.

The Influence of PAA Addition on HER Activity of the Cathode

The HER catalytic performances of the NF@Pt/C cathode in electrolytes without PAA and with PAA were tested (Figure 7A). The onset overpotential of NF@Pt/C in PAA-added electrolyte is 25.8 mV, which is lower than that of NF@Pt/C in electrolyte without PAA (56.51 mV). In addition, the cathode tested with PAA requires an overpotential of only 87.78 mV to achieve a current density of 10 mA cm^{-2}. This value is much lower than that required by the cathode at 10 mA cm^{-2} without PAA (247.03 mV). Therefore, the addition of PAA to the electrolyte significantly increases the catalytic activity of the cathode.

Figure 7B shows the Tafel plots of the cathode for HER in electrolytes with and without PAA. NF@Pt/C exhibits a Tafel

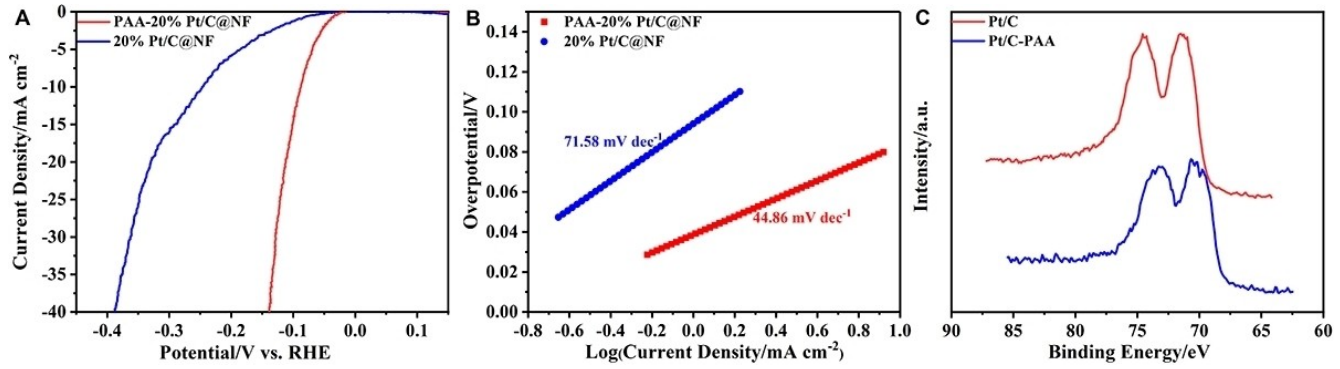

Figure 7. LSV curves (A) and Tafel plots (B) of the NF@Pt/C electrode for HER measured in simulated seawater with and without PAA and high-resolution Pt 4f XPS spectra of NF@Pt/C with and without PAA adsorption (C).

Research Article
doi.org/10.1002/batt.202400307
Chemistry Europe
European Chemical Societies Publishing

slope of 71.58 mV dec^{-1} in electrolyte without PAA. In comparison, the Tafel slope for NF@Pt/C in PAA-added electrolyte is 44.86 mV dec^{-1}. This result indicates that PAA greatly improves the HER kinetics of the cathode.

The electronic structures of the Pt/C catalysts modified with PAA and without modification was investigated via XPS for revealing the possible mechanism for the enhanced HER activity in PAA-added electrolyte. The high-resolution Pt 4f XPS spectra show that the binding energy of Pt $4f_{7/2}$ in NF@Pt/C after adsorption of PAA in PAA-added electrolyte is 70.68 eV, which is 0.8 eV lower than that of Pt metal in NF@Pt/C without PAA adsorption (71.48 eV) (Figure 7C). The reduced binding energy of Pt is caused by PAA donating electrons to Pt via coordination. The electron donation to Pt shifts the d-band center of Pt downward, thus reducing its binding strength with H, which is favorable to enhance the HER activity under alkaline conditions.[20] In addition, the adsorption of PAA on Pt will provide a more acidic environment near the active sites for higher HER efficiency.[25,26]

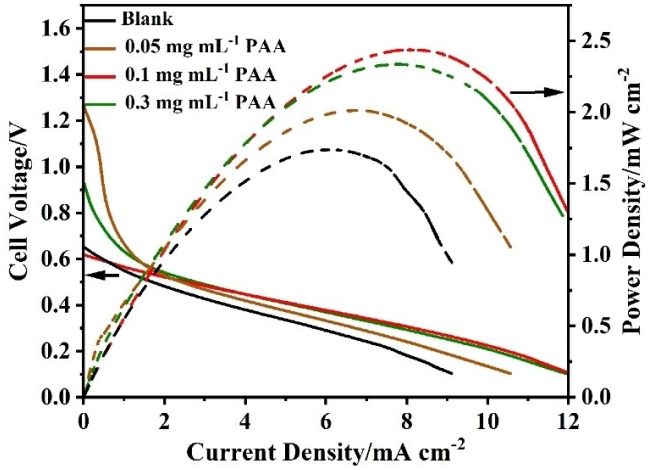

Figure 8. Polarization curves and corresponding power density curves of Al/H_2O batteries with different concentrations of PAA in simulated seawater.

The Influence of PAA Concentration on Power Density

With the unique dual function of PAA to simultaneously inhibit the self-corrosion of Al anode and increase the HER activity of the NF@Pt/C cathode, it is thus desirable to optimize its concentration for enhancing the battery performance. The polarization curves of Al/H_2O batteries with pure Al as the anode, NF@Pt/C as the cathode, and different concentrations of PAA in simulated seawater (with pH adjusted to 12 and with PAA of different concentrations added) as the electrolyte are shown in Figure 8. With the increase of the PAA concentration from 0.05 to 0.1 mg mL^{-1}, the power density increases. However, further increasing PAA concentration to 0.3 mg mL^{-1} leads to a decrease of the power density. The increase of power density when increasing the PAA concentration from 0 to 0.1 mg mL^{-1} is attributed to the PAA molecules inhibiting self-corrosion of Al anode and enhancing HER activity of the cathode. The decrease of power density at a high PAA concentration is due to the formation of a too thick layer of PAA-Al^{3+} on the Al anode surface inhibiting the exposure of active sites to the electrolyte. Combining the power density and anode utilization efficiency data (Figure 2), the optimum PAA concentration is 0.1 mg mL^{-1}, which ensures a high power density of the battery and a high utilization of the anode.

Performance Optimization With Al-Bi-Pb-Ga Alloy

It has been reported that doping of slight amount of Bi, Pb, and Ga can improve the anode efficiency of Al.[9,27] To further improve the performance of Al/H_2O batteries for practical applications, Al-0.15Bi-0.15Pb-0.035Ga, which has been regarded as one of the best Al anodes,[9] is adopted as the anode to replace Al. The optimized modified simulated seawater (3.5% NaCl, pH 12, and 0.1 mg mL^{-1} PAA) is used as the electrolyte of the Al/H_2O battery. The battery shows a significantly improved performance, with a power density of 20.87 mW cm^{-2}, an anode efficiency of 76.2%, and a specific energy density of 2271 Wh kg^{-1} (Figure 9). This performance is much higher than Mg/H_2O batteries,[28] which are recognized to have the greatest potential for UUV applications.[1,29] The energy density is also the highest among those of all the reported batteries.[28] In

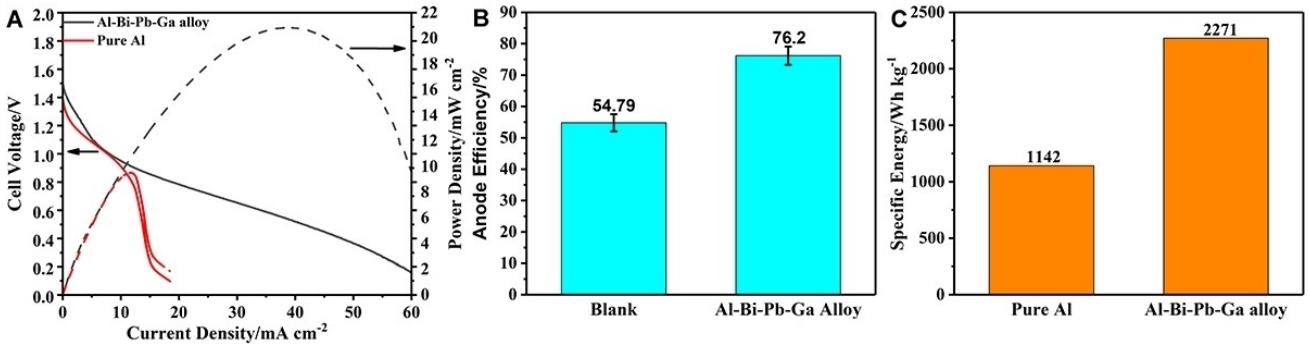

Figure 9. Polarization curves and corresponding power density curves (A), anode efficiencies for 10 h of discharge at 2 mA cm^{-2} (B), and energy density (C) of Al/H_2O batteries with different anodes.

addition, the power density is highest reported for metal/H_2O batteries.[30]

Conclusions

For the first time, a type of Al/H_2O batteries has been developed with electrolyte made of simulated seawater at an appropriate pH and added with PAA. It has been discovered that the electrolyte simultaneously greatly retards the self-corrosion of the Al anode by in situ forming a PAA-Al^{3+} complex film on the anode and increases the electrocatalytic activity toward the HER by improving the electronic structure via electron transfer from PAA to Pt. When utilizing the multielement-doped Al sheet as the anode and the nickel foam supported loading-amount-optimized Pt/C catalyst as the cathode and adopting the developed new electrolyte, the obtained Al/H_2O battery exhibits an energy density of 2271 Wh kg^{-1}, which is the highest among those of all the reported batteries, and a power density of 20.87 mW cm^{-2}, which outperforms all the reported metal/H_2O batteries. This work not only provides an effective, facile, and economical strategy to improve both the anode and cathode efficiency for enhanced Al/H_2O battery performance toward the UUV applications, but sheds light on the design of superior electrolytes, which could be further extended for improving the performance of various metal batteries. The exploration of using actual seawater to prepare the electrolyte for the Al/H_2O batteries is ongoing in our lab with promising preliminary results and will be published in the near future.

Experimental Section

Materials

Al sheets (99.99%), Nafion (5%), and PAA (average M_v ~450000) were obtained from Aladdin. Pt/C was purchased from Shanghai Hesen Electric Co. NF and Al–Bi–Pb–Ga alloy were purchased from Suzhou keshenghe Co. and Beijing Yijinxincai Co. The deionized water was produced via a Milli-Q water purification system (Millipore).

Preparation of Electrodes and Electrolyte

The anode was a pure aluminum or doped Al sheet of 20 mm×10 mm×1 mm.

For the preparation of the cathode, commercial Pt/C was dispersed in ethanol via sonication. Nafion was then added into the suspension (the weight ratio of Pt/C to Nafion is 4 : 1) and further sonicated. The catalyst suspension was subsequently drop-casted on NF (the loading is 200 μg cm^{-2}).

For the preparation of the electrolyte, NaCl (3.5%) and PAA of different concentrations were added into deionized water. The pH of the solution was then adjusted to 12 with 1 M KOH.

Electrochemical Measurements

The batteries were tested in the two-electrode setup using an electrochemical workstation (CHI 760E). The anode and cathode were both submerged in the electrolyte (the volume is 50 mL) with an area of 1 cm×1 cm. The spacing between electrodes is 15 mm. For maintaining the pH of the electrolyte during the testing, the cell was well sealed only allowing the produced H_2 to diffuse out. The performance was measured using LSV (scan rate: 5 mV s^{-1}).

A battery test system (CT-4008T-5V10mA, Neware) was used to test the constant current discharge of Al/H_2O batteries. The anode and cathode were submerged in the electrolyte (the volume is 50 mL) with an area of 1 cm×1 cm and an electrode spacing of 15 mm. The power density curves of Al/H_2O batteries were obtained by multiplying current and voltage measured via LSV. The anode efficiency is calculated by the differential weight method using the following equation:[9,31]

$$\eta = \frac{It}{mC} \times 100\,\%$$

where η is the anode utilization rate, I the magnitude of the discharge current, t the discharge time, m the difference in mass of the aluminum anodes before and after discharge, and C the electrochemical equivalent. Specific energy, which represents the amount of electrical energy released per unit mass of battery, can be calculated by the following equation:[28,32]

$$E = \frac{CU}{M}$$

where E is specific energy, C cell capacity, U voltage, and M Al mass.

Supporting Information

Supporting Information is available from the Wiley Online Library or from the author.

Acknowledgements

This work was financially supported by the Yongjiang Talent Introduction Programme (Grant No. 2021A-155-G), National Natural Science Foundation of China (No. 52205074), Natural Science Foundation of Ningbo, China (Grant No. 2022J156), and Start-up Grant from Zhejiang University, China (Grant No. 1140457B20210129).

Conflict of Interests

The authors declare no conflict of interest.

Data Availability Statement

The data that support the findings of this study are available from the corresponding author upon reasonable request.

Keywords: underwater unmanned vehicles · Al/seawater batteries · self-corrosion inhibitors · hydrogen evolution reaction catalysts · specific energy

[1] X. Wang, J. Shang, Z. Luo, L. Tang, X. Zhang, J. Li, *Renew. Sust. Energ. Rev.* **2012**, *16*, 1958–1970.
[2] M. Shinohara, E. Araki, M. Mochizuki, T. Kanazawa, K. Suyehiro, *J. Power Sources* **2009**, *187*, 253–260.
[3] X. Liu, H. Jiao, M. Wang, W. Song, J. Xue, S. Jiao, *Int. Mater. Rev.* **2021**, *67*, 734–764.
[4] J. M. Bergthorson, Y. Yavor, J. Palecka, W. Georges, M. Soo, J. Vickery, S. Goroshin, D. L. Frost, A. J. Higgins, *Appl. Energy* **2017**, *186*, 13–27.
[5] Y. Xu, J. Ma, T. Jiang, H. Ding, W. Wang, M. Wang, X. Zheng, J. Sun, Y. Yuan, M. Chuai, N. Chen, Z. Li, H. Hu, W. Chen, *Energy Storage Mater.* **2022**, *47*, 113–121.
[6] Z. Ma, X. Li, *J. Solid State Chem.* **2011**, *15*, 2601–2610.
[7] D. J. Brodrecht, J. J. Rusek, *Appl. Energy* **2003**, *74*, 113–124.
[8] G. Fotouhi, C. Ogier, J.-H. Kim, S. Kim, G. Cao, A. Q. Shen, J. Kramlich, J.-H. Chung, *J. Micromech. Microeng.* **2016**, *26*, 055011.
[9] Q. Wang, H. Miao, Y. Xue, S. Sun, S. Li, Z. Liu, *RSC Adv.* **2017**, *7*, 25838–25847.
[10] Q. Li, N. J. Bjerrum, *J. Power Sources* **2002**, *110*, 1–10.
[11] P. Wu, S. Wu, D. Sun, Y. Tang, H. Wang, *Acta Metall. Sin.* **2021**, *34*, 309–320.
[12] L. Huang, Y. Hou, Z. Yu, Z. Peng, L. Wang, J. Huang, B. Zhang, L. Qian, L. Wu, Z. Li, *Int. J. Hydrogen Energy* **2017**, *42*, 9458–9466.
[13] P. K. Shen, A. C. C. Tseung, C. Kuo, *J. Power Sources* **1994**, *47*, 119–127.
[14] P. K. Shen, A. C. C. Tseung, C. Kuo, *J. Appl. Electrochem.* **1994**, *24*, 145–148.
[15] K. A. Yasakau, J. Tedim, M. L. Zheludkevich, R. Drumm, M. Shem, M. Wittmar, M. Veith, M. G. S. Ferreira, *Corros. Sci.* **2012**, *58*, 41–51.
[16] M. A. Deyab, Q. Mohsen, *Electrochim. Acta* **2017**, *244*, 178–183.
[17] S. Wu, Q. Zhang, D. Sun, J. Luan, H. Shi, S. Hu, Y. Tang, H. Wang, *Chem. Eng. J.* **2020**, *383*, 123162.
[18] Y. Liu, H. Zhang, Y. Liu, J. Li, W. Li, *J. Power Sources* **2019**, *434*, 226723.
[19] T. Li, X. Wang, W. Yuan, C. M. Li *ChemElectroChem* **2016**, *3*, 204–208.
[20] B. Hammer, J. K. Nrskov, *Adv. Catal.* **2000**, *45*, 71–129.
[21] Z. Zhang, C. Zuo, Z. Liu, Y. Yu, Y. Zuo, Y. Song, *J. Power Sources* **2014**, *251*, 470–475.
[22] S. Anjum, P. Gurave, M. V. Badiger, A. Torris, N. Tiwari, B. Gupta, *Polymer* **2017**, *126*, 196–205.
[23] M. A. Amin, S. S. A. Ei-Rehim, E. E. F. El-Sherbini, O. A. Hazzazi, M. N. Abbas, *Corros. Sci.* **2009**, *51*, 658–667.
[24] A. V. Dobrynin, M. Rubinstein, *Prog. Polym. Sci.* **2005**, *30*, 1049–1118.
[25] H. Tan, B. Tang, Y. Lu, Q. Ji, L. Lv, H. Duan, N. Li, Y. Wang, S. Feng, Z. Li, C. Wang, F. Hu, Z. Sun, W. Yan, *Nat. Commun.* **2022**, *13*, 2024.
[26] S. Lu, T. Zhang, *Chem Catal.* **2022**, *2*, 1505–1509.
[27] P. Wu, S. Wu, D. Sun, Y. Tang, H. Wang, *Acta Metall. Sin.* **2021**, *34*, 309–320.
[28] Q. Liu, Z. Yan, E. Wang, S. Wang, G. Sun, *Int. J. Hydrogen Energy* **2017**, *42*, 23045–23053.
[29] W. Kohnen, *MTS J.* **2013**, *47*, 56–68.
[30] Y. Xu, H. Lv, H. Lu, Q. Quan, W. Li, X. Cui, G. Liu, L. Jiang, *Nano Energy* **2022**, *98*, 107295.
[31] J. Ma, G. Wang, Y. Li, F. Ren, A. A. Volinsky, *Ionics* **2019**, *25*, 2201–2209.
[32] X. Liu, S. Liu, J. Xue, *J. Power Sources* **2018**, *396*, 667–674.

Manuscript received: May 6, 2024
Revised manuscript received: June 25, 2024
Accepted manuscript online: June 27, 2024
Version of record online: August 12, 2024